

1 Drug synergy of combinatory treatment with remdesivir and the repurposed drugs fluoxetine
2 and itraconazole effectively impairs SARS-CoV-2 infection in vitro.

3 Sebastian Schloer¹, Linda Brunotte², Angeles Mecate-Zambrano², Shuyu Zheng³, Jing
4 Tang³, Stephan Ludwig², Ursula Rescher^{1*}

5 ¹Institute of Medical Biochemistry, Center for Molecular Biology of Inflammation, and “Cells
6 in Motion” Interfaculty Centre, University of Muenster, Von-Esmarch-Str. 56, D-48149,
7 Muenster, Germany

8 ²Institute of Molecular Virology, Center for Molecular Biology of Inflammation, and “Cells in
9 Motion” Interfaculty Centre, University of Muenster, Von-Esmarch-Str. 56, D-48149,
10 Muenster, Germany

11 ³Research Program in Systems Oncology, Faculty of Medicine, University of Helsinki,
12 Haartmaninkatu 8, 00029, Helsinki, Finland

13 *Correspondence: Ursula Rescher, rescher@uni-muenster.de, Tel. +492518352118, Fax.
14 +492518356748

15 running title: Combinatory drug treatment targeting both virus and host-factors to inhibit
16 SARS-CoV-2 infection

17 ABSTRACT

18 The SARS-CoV-2 pandemic and the global spread of coronavirus disease 2019
19 (COVID-19) urgently calls for efficient and safe antiviral treatment strategies. A
20 straightforward approach to speed up drug development at lower costs is drug repurposing.
21 Here we investigated the therapeutic potential of targeting the host- SARS-CoV-2 interface
22 via repurposing of clinically licensed drugs and evaluated their use in combinatory
23 treatments with virus- and host-directed drugs. We tested the antiviral potential of
24 repurposing the antifungal itraconazole and the antidepressant fluoxetine on the production
25 of infectious SARS-CoV-2 particles in the polarized Calu-3 cell culture model and evaluated
26 the added benefit of a combinatory use of these host-directed drugs with remdesivir, an
27 inhibitor of viral RNA polymerase. Drug treatments were well-tolerated and potent impaired
28 viral replication was observed with all drug treatments. Importantly, both

29 itraconazole-remdesivir and fluoxetine-remdesivir combinations inhibited the production of
30 infectious SARS-CoV-2 particles > 90% and displayed synergistic effects in commonly used
31 reference models for drug interaction. Itraconazole-Remdesivir and Fluoxetine-Remdesivir
32 combinations are promising therapeutic options to control SARS-CoV-2 infection and severe
33 progression of COVID-19.

34 **1. INTRODUCTION**

35 The zoonotic coronavirus SARS-CoV-2 and the resulting COVID-19 pandemic impressively
36 show the global threat potential of a newly emerging pathogen. More than one million people
37 have died so far from the current outbreak, and the proportion of infected people was
38 estimated to reach more than 10% of the global population, with still unknown fatality rates
39 (Baud et al., 2020; Rajgor et al., 2020; Wu et al., 2020). Because of the pressing burden on
40 national health systems and economic losses, safe and efficient treatment strategies are
41 urgently required. Developing a vaccine is a high priority. However, the rigorous testing and
42 extensive clinical trials are time-consuming processes. While several trials are already
43 ongoing, there are no vaccines available yet, and the required widespread access remains a
44 challenging future task. Thus, approaches other than immunization might offer useful
45 additional options for the management and control of SARS-CoV-2 infection and the
46 treatment of COVID-19 (Fierabracci et al., 2020). A possibility to speed up the availability of
47 drugs for the treatment of novel infections is the use of drugs that are already in clinical use
48 for unrelated diseases via so-called "drug repurposing". This approach represents a
49 promising strategy to identify antiviral drugs with faster clinical implementation and lower
50 development costs, considerations that are especially important in the global COVID-19
51 pandemic (Pushpakom et al., 2018). In addition to drugs that directly target the virus, host
52 cell components that are vitally important in the viral life cycle are explored as promising
53 starting points for therapeutic intervention ("host cell-directed therapy") (Schwegmann and
54 Brombacher, 2008; Ianevski et al., 2020; Zumla et al., 2020).

55 Although proteolytic cleavage of the SARS-CoV-2 spike protein surface protein by the host
56 cell transmembrane protease serine 2 (TMPRSS2) enables SARS-CoV-2 to directly fuse
57 with the plasma membrane, endocytosed SARS-CoV-2 particles use endosome-residing
58 proteases for fusion within endosomes (Tang et al., 2020). Both pathways contribute to the
59 SARS-CoV-2 infection process, and the preferential use of the actual fusion pathway might
60 critically depend on the presence of plasma membrane proteases (Hoffmann et al., 2020).
61 Our earlier research on influenza virus infection identified the late endosomal cholesterol
62 balance as a critical factor in the influenza infection success and established this viral entry
63 point as a possible pharmacological target. Elevated cholesterol levels inhibit the fusion of
64 the influenza lipid hull with the endosomal membranes and thus inhibit the efficient transfer
65 of the viral genome into the host cytosol (Musiol et al., 2013; Kühnl et al., 2018). We found
66 that the clinically licensed antifungal itraconazole, a triazole derivative that blocks the fungal
67 ergosterol pathway, has antiviral properties against a range of viruses and is effective
68 against IAV infections in a preclinical mouse model (Schloer et al., 2019, 2020b). The
69 additional therapeutic function is most likely based on direct inhibition of the endosomal
70 cholesterol transporter Niemann-Pick Type C1 (NPC1) and the subsequent cholesterol
71 storage ((Trinh et al., 2017; Schloer et al., 2019)).

72 The late endosome is an entry site for many zoonotically transmitted viruses, in particular for
73 enveloped viruses including SARS-CoV-2 (Tang et al., 2020). Because of the functional
74 similarities in transmitting the viral genome into the host cell, the same endosomal
75 components might serve as pharmacological targets for a broad host-directed antiviral
76 strategy against such viruses. Continuing our work on the endosomal host-virus interface,
77 we explored whether a similar repurposing strategy could be used to impair SARS-CoV-2
78 entry and infection. Therefore, we assessed clinically licensed drugs that also affect
79 endolysosomal lipid storage and cholesterol build-up for their antiviral potential. Here we
80 report that itraconazole treatment potently inhibited the production of SARS-CoV-2
81 infectious particles. Together with our recently published work on the antiviral potential of the
82 widely used serotonin inhibitor fluoxetine, which also negatively affects endosomal

83 cholesterol release (Kornhuber et al., 2010; Schloer et al., 2020a) on SARS-CoV-2 infection,
84 the results presented in this study strongly argue for the endolysosomal host-SARs-CoV-2
85 interface as a druggable target. However, host-directed drugs will rather suppress infection
86 than completely eradicate the pathogen. The resulting demand for high drug doses and
87 early and prolonged treatment is often associated with poor patient compliance. While drugs
88 directly acting on virus structures are much more likely to completely eliminate the
89 pathogens in shorter treatment time, emerging viral resistance to these antivirals is a major
90 concern, as observed with the influenza neuraminidase inhibitor oseltamivir (Kim et al.,
91 2013). Thus, combination therapies using virus- and host-directed drugs are considered to
92 overcome these shortcomings. The nucleoside analog remdesivir which was originally
93 developed against Ebola (Warren et al., 2016), has antiviral properties with a broad
94 spectrum of activity against a number of RNA viruses and has already been shown to be
95 effective against SARS and Mers-CoV in animal experiments (Sheahan et al., 2017, 2020;
96 Agostini et al., 2018; Pruijssers et al., 2020). When remdesivir is incorporated into the viral
97 RNA, the synthesis is prematurely terminated, and viral replication is inhibited (Gordon et al.,
98 2020). Therefore, we explored combined treatments with remdesivir and the repurposed
99 drugs itraconazole and fluoxetine. Both drug combinations showed stronger antiviral
100 activities against influenza viruses compared to remdesivir monotherapy (Schloer et al.,
101 2020b). Importantly, the antiviral effects of the combined treatments deviated from the
102 expected effects, and pharmacodynamic evaluation via commonly used reference models to
103 study drug interaction revealed synergistic interaction.

104 **2. MATERIALS AND METHODS**

105 **2.1 Cells and SARS-CoV-2 isolate**

106 The human bronchial epithelial cell lines Calu-3 and the Vero E6 cells were cultivated in
107 Dulbecco's modified Eagle's medium (DMEM) with 10% standardized fetal bovine serum
108 (FBS Superior; Merck), 2 mM L-glutamine, 100 U/mL penicillin, 0.1 mg/mL streptomycin,
109 and 1% non-essential amino acids (Merck) in a humidified incubator at 5% CO₂ and 37 °C.
110 Calu-3 monolayers were polarized and cultured as described (Schloer et al., 2020b).

111 Itraconazole (2 mg/mL, Sigma), fluoxetine (5 mM, Sigma) and remdesivir (10 mM, Hycultec)
112 were solubilized in DMSO. The SARS-CoV-2 isolate hCoV-19/Germany/FI1103201/2020
113 (EPI-ISL_463008, mutation D614G in spike protein) was amplified on Vero E6 cells and
114 used for the infection assays.

115 **2.2 Cytotoxicity assay**

116 Calu-3 cells were cultured at the indicated concentrations with either the solvent DMSO,
117 itraconazole or with the combinations of itraconazole/ remdesivir (ItraRem) or fluoxetine/
118 remdesivir (FluoRem) for 48 h. Staurosporine solution (1 μ M) served as a positive control for
119 cytotoxic effects. After 48 hours of treatment, cell viability was evaluated by adding MTT
120 3-(4,5-dimethylthiazol-2-yl)-2,5-diphenyltetrazolium bromide (Sigma) to the cells for 4 h and
121 OD₅₆₂ measurements according to the manufacturer's protocols (Sigma).

122 **2.3 Inoculation of cells and drug treatment**

123 For infection, polarized Calu-3 and Vero cells were washed with PBS and inoculated at a
124 multiplicity of infection (MOI) of 0.1 (Calu-3) or 0.01 (Vero E6) of virus diluted in
125 infection-PBS (containing 0.2% BSA, 1% CaCl₂, 1% MgCl₂, 100 U/mL penicillin and 0.1
126 mg/mL streptomycin) at 37°C for 1 hours. Subsequently, cells were washed with PBS and
127 further cultured in infection-DMEM (serum-free DMEM containing 0.2% BSA, 1 mM MgCl₂,
128 0.9 mM CaCl₂, 100 U/mL penicillin, and 0.1 mg/mL streptomycin) at 5% CO₂ and 37 °C.
129 Cells were treated with the indicated remdesivir, itraconazole or fluoxetine concentration 2
130 hours post-infection (hpi) for the entire 48 hours infection period. After 48 hpi, apical culture
131 supernatants were collected and immediately frozen at -80 °C until titration via plaque
132 assay.

133 **2.4 Plaque assay**

134 To determine the number of infectious particles in the supernatant of treated cells, a
135 standard plaque assay was performed. Briefly, Vero E6 cells grown to a monolayer in
136 six-well dishes were washed with PBS and infected with serial dilutions of the respective
137 supernatants in infection-PBS for 1 hour at 37 °C. The inoculum was replaced with 2x MEM

138 (MEM containing 0.2% BSA, 2 mM L-glutamine 1 M HEPES, pH 7.2, 7.5% NaHCO₃, 100
139 U/mL penicillin, 0.1 mg/mL streptomycin, and 0.4% Oxoid agar) and incubated at 37°C.
140 Virus plaques were visualized by staining with neutral red, and virus titers were calculated as
141 plaque-forming units (PFU) per mL.

142 **2.5 Data and statistical analysis**

143 A priori power analysis using G*Power 3.1 (Faul et al., 2007)) was performed to determine
144 the sample sizes required to detect > 90% reduction in virus titers at powers > 0.8. Data
145 were analyzed using the software GraphPad Prism version 8.00 (GraphPad). No outliers
146 were detected.

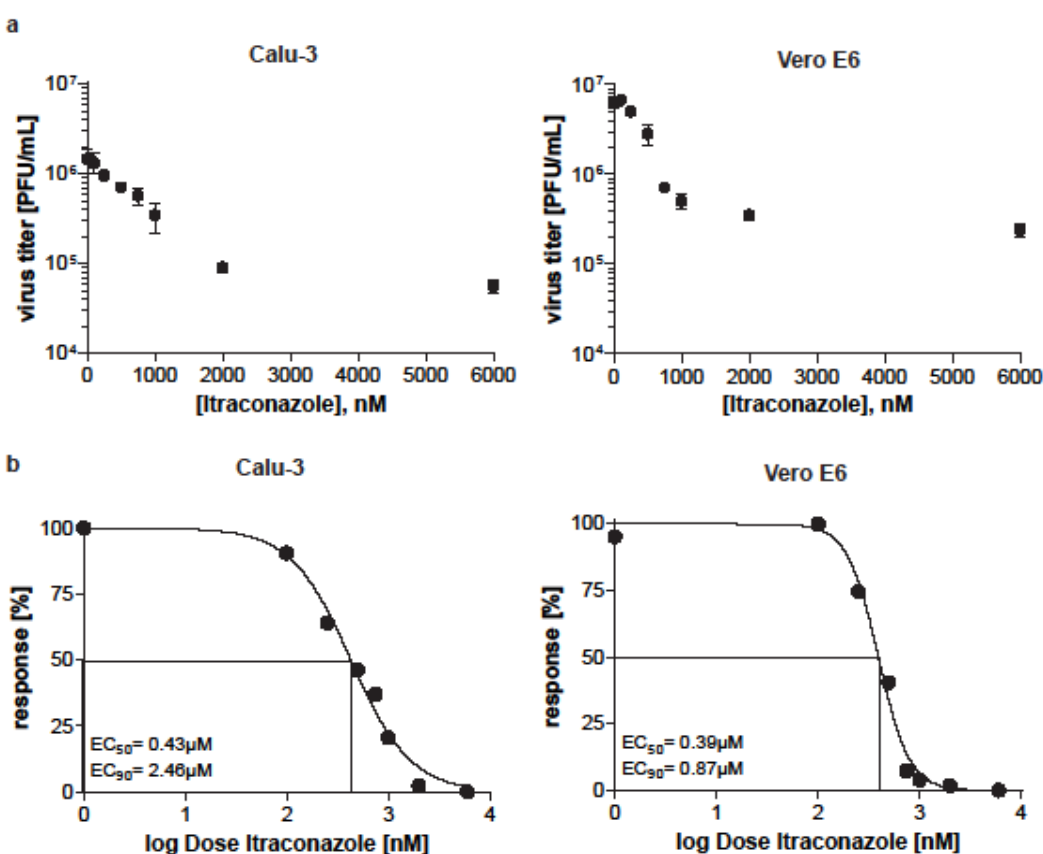
147 Infectious viral titers are presented as means \pm SEM of five measurements per
148 experiment per condition. For dose-response curves, drug concentrations were
149 log-transformed and virus titers were expressed as percentages of the mean virus titer in
150 control cells (treated with the solvent DMSO) and data were analyzed by curve fitting using a
151 4 parameter logistic model. Drug combinatory effects were analyzed by using
152 SynergyFinder, an open-source free stand-alone web application for the analysis of drug
153 combination data (Ianevski et al., 2017). Synergy was evaluated based on the Zero
154 Interaction Potency (ZIP), Bliss independence, and Highest single agent (HSA) reference
155 models (He et al., 2018). We further analyzed the overall drug combination sensitivity score
156 (CSS) by using the CSS method (Malyutina et al., 2019).

157 **3. RESULTS**

158 **3.1. The clinically licensed antifungal drug itraconazole efficiently blocks the
159 production of SARS-CoV-2 infectious particles**

160 Based on the successful use of repurposing itraconazole for the treatment of influenza virus
161 infection reported in our earlier studies (Schloer et al., 2019, 2020b), we first established
162 whether this clinically licensed drug also had an antiviral potential on the production of
163 infectious SARS-CoV-2 particles. In line with our previous results (Schloer et al., 2020a),
164 both Calu-3 and Vero E6 cell lines supported SARS-CoV-2 replication and produced high

165 virus titers (Fig. 1). Inoculation with the clinical isolate hCoV-19/Germany/FI1103201/2020
166 at MOI 0.1 yielded 1.46×10^6 PFU in Calu-3 cells and 6.37×10^6 PFU at MOI 0.01 in Vero cells
167 at 48 hpi. Treatment with itraconazole 2 hpi potently inhibited SARS-CoV-2 replication in a
168 dose-dependent manner in both cell types (Fig. 1a). Fitting the experimental dose-response
169 values to a nonlinear 4 parameter logistic model revealed half-maximal inhibitory (EC_{50}) and
170 90% inhibitory concentrations (EC_{90}) of 0.43 μ M and 2.46 μ M in Calu-3 cells, and even lower
171 50% and 90% inhibitory concentrations (0.39 μ M and 0.87 μ M) were determined for
172 itraconazole antiviral activity in SARS-CoV-2 infected Vero cells (Fig. 1b). Of note, no
173 detectable cytotoxicity was observed with these doses (Fig. S1a). The itraconazole cytotoxic
174 concentration required to reduce cell viability by 50% (CC_{50}) was determined at 25.56 μ M,
175 resulting in a selectivity index (SI, defined as the ratio of CC_{50} to EC_{50}) of 25.56 μ M which
176 indicated an effective and safe antiviral window.



177
178 **FIGURE 1** Analysis of itraconazole-mediated reduction of SARS-CoV-2 replication. Calu-3
179 and Vero E6 cells were infected with 0.1 MOI of SARS-CoV-2. At 2 hpi, cells were treated
180 with itraconazole at the indicated concentrations. (a) Mean infectious viral titers \pm SEM,

181 (b) Mean percent inhibition \pm SEM of SARS-CoV-2 replication, with mean virus titer in
182 control cells (treated with the solvent DMSO) set to 100%; n = 5. LogEC₅₀ and LogEC₉₀
183 values were determined by fitting a non-linear regression model. (Calu-3: EC₅₀ = 0.43 μ M,
184 EC₉₀ = 2.46 μ M; Vero E6: EC₅₀ = 0.39 μ M, EC₉₀ = 0.87 μ M).

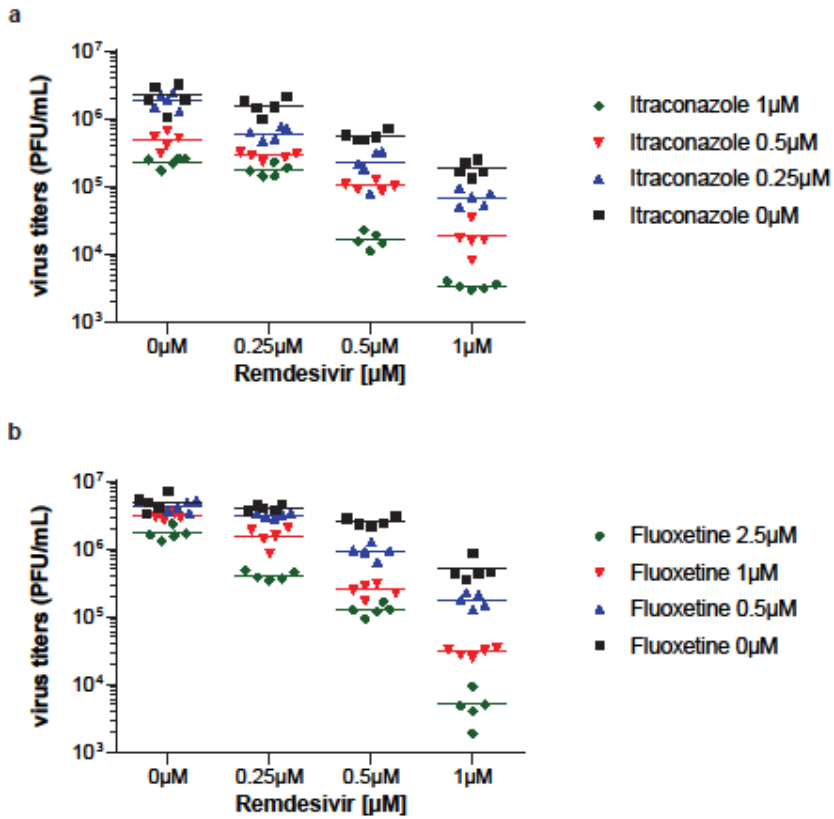
185 **3.2 Remdesivir inhibits SARS-CoV-2 replication in polarized Calu-3 cells**

186 We addressed the question of whether a host-targeting drug could be used in combination
187 with a virus-directed drug for more efficient suppression of SARS-CoV-2 replication. Thus,
188 we first assessed the antiviral capacity of remdesivir, a nucleotide analog prodrug that
189 inhibits SARS-CoV-2 viral RNA-dependent RNA polymerase (Gordon et al., 2020). The
190 EC₅₀ concentration was reached at 0.42 μ M and EC₉₀ at 1.08 μ M in Calu-3 cells (Fig. S2),
191 well in line with published data (Pruijssers et al., 2020). Next, we determined viral replication
192 in cells that had been treated with combinatory therapy. Because we recently published the
193 potential use of repurposing the antidepressant fluoxetine for treatment of SARS-CoV-2
194 infection (Schloer et al., 2020a), we also assessed the effects of a combined
195 fluoxetine/remdesivir (FluoRem) treatment in addition to the itraconazole/remdesivir
196 (ItraRem) combination (Fig. 2). Both drugs are clinically licensed and do not induce
197 significant cytotoxicity over the whole concentration range ((Schloer et al., 2020a), and Fig.
198 S1a). The combination treatments were also well-tolerated, and no cytotoxic effects were
199 seen when cells were simultaneously treated with the drug pairs (Fig. S1b, c).

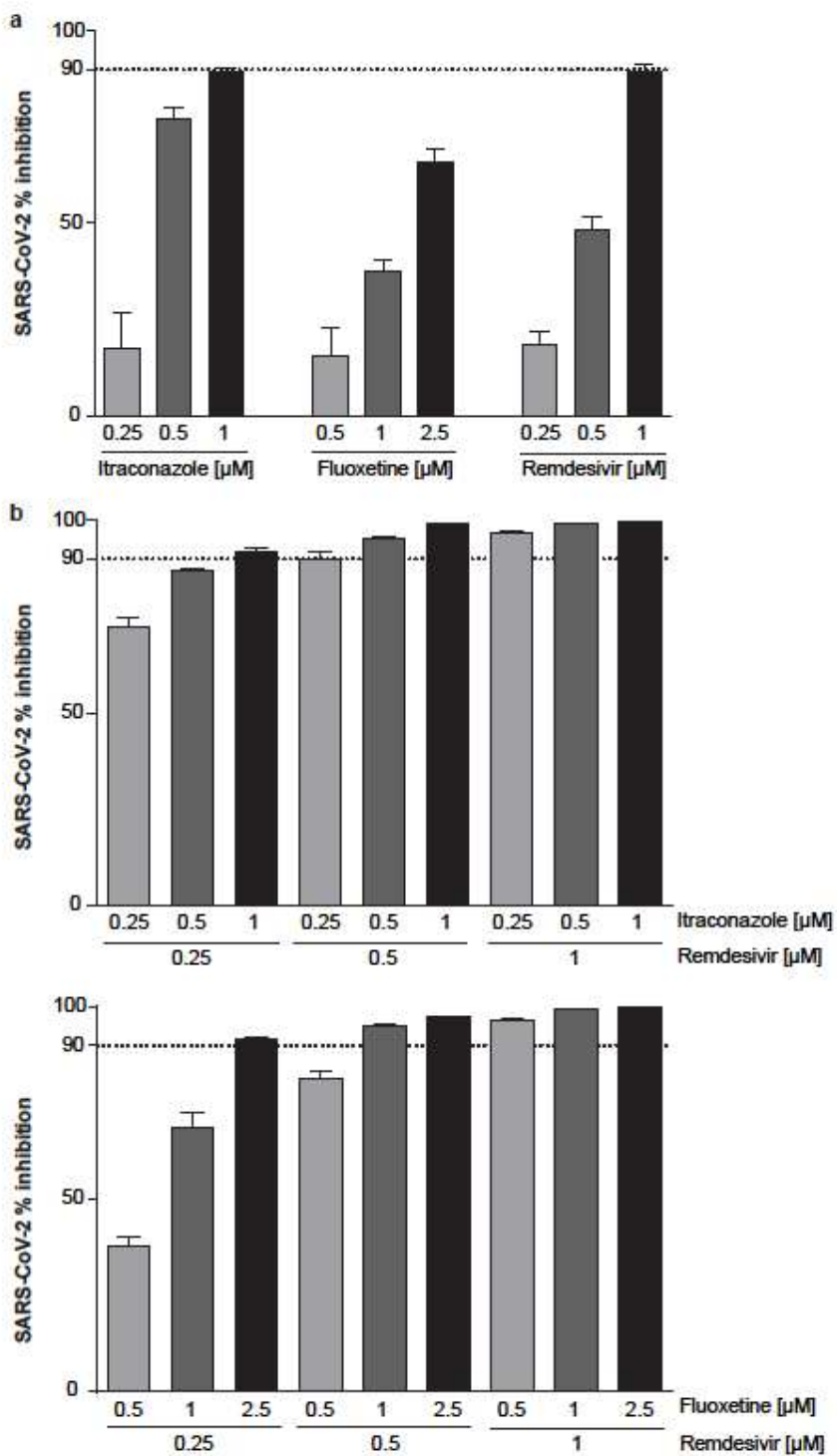
200 **3.3 Combinatory treatments with the drug pairs itraconazole-remdesivir or**

201 **fluoxetine-remdesivir show enhanced antiviral activity due to synergistic interaction**

202 For all drugs, we chose those concentrations that were not sufficient to achieve a 90%
203 reduction when individually applied (Fig 3a). For both ItraRem and FluoRem combinations, a
204 potent reduction in virus titers was detected in all cases. Of note, several combinations
205 yielded a reduction > 90% of the maximum virus titers produced in control cells (Fig. 3b).

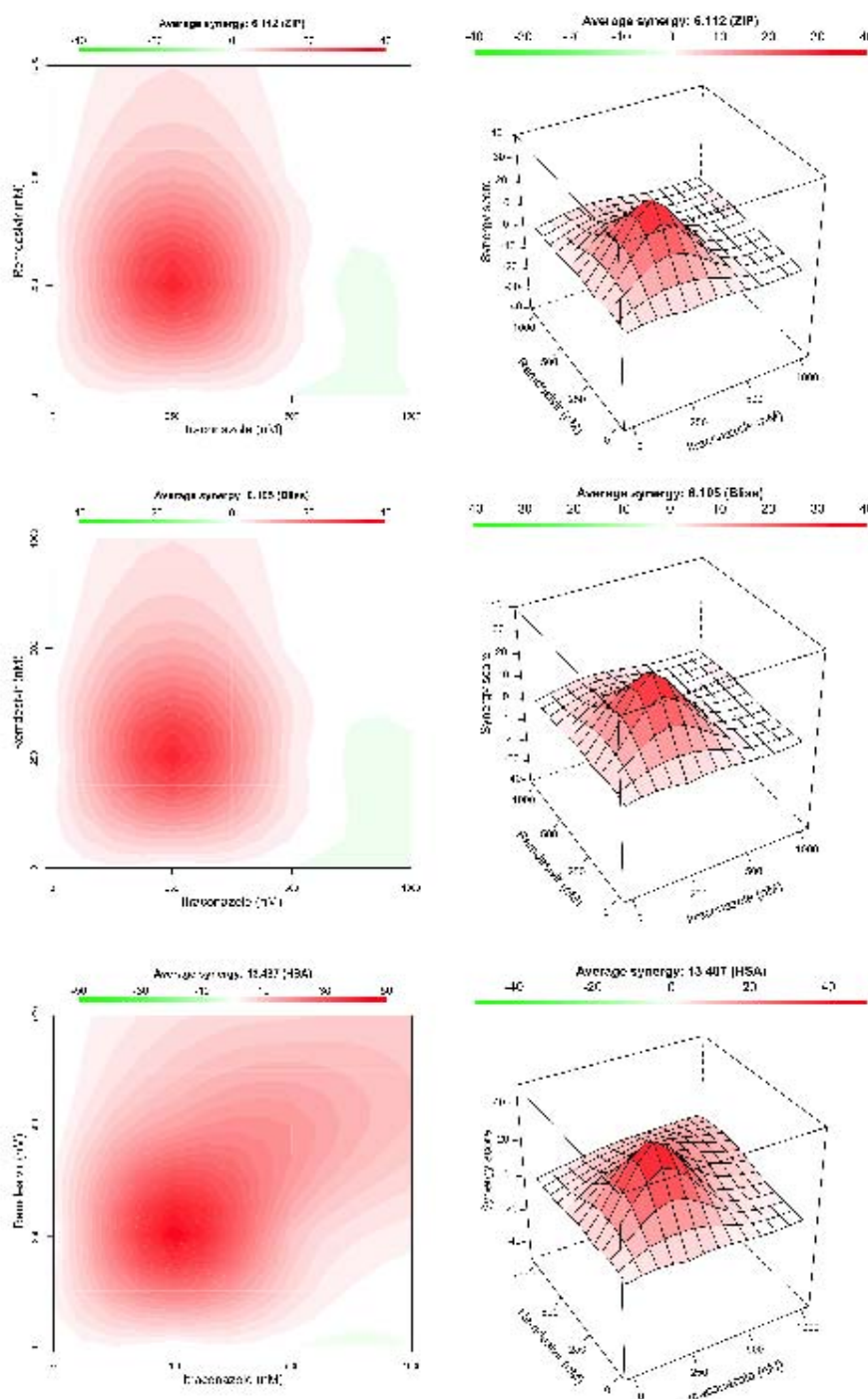


206
207 **FIGURE 2** Antiviral activities of treatments. Infectious virus production in Calu-3 cells treated
208 as indicated 2 hpi. Each symbol represents plaque-forming units (PFU) per mL detected in a
209 single experimental sample, lines indicate means.



210
211 **FIGURE 3** Antiviral activities of single and combination treatments. Calu-3 cells were treated
212 with the indicated drug combinations for 48 h. (a) Single treatment, (b) combinatory
213 treatment. Bars represent mean percent inhibition \pm SEM of infectious virus production,
214 with mean virus titer produced in control cells (treated with the solvent DMSO) set to 100%;
215 n = 5. Dotted line, 90% reduction in viral titer.

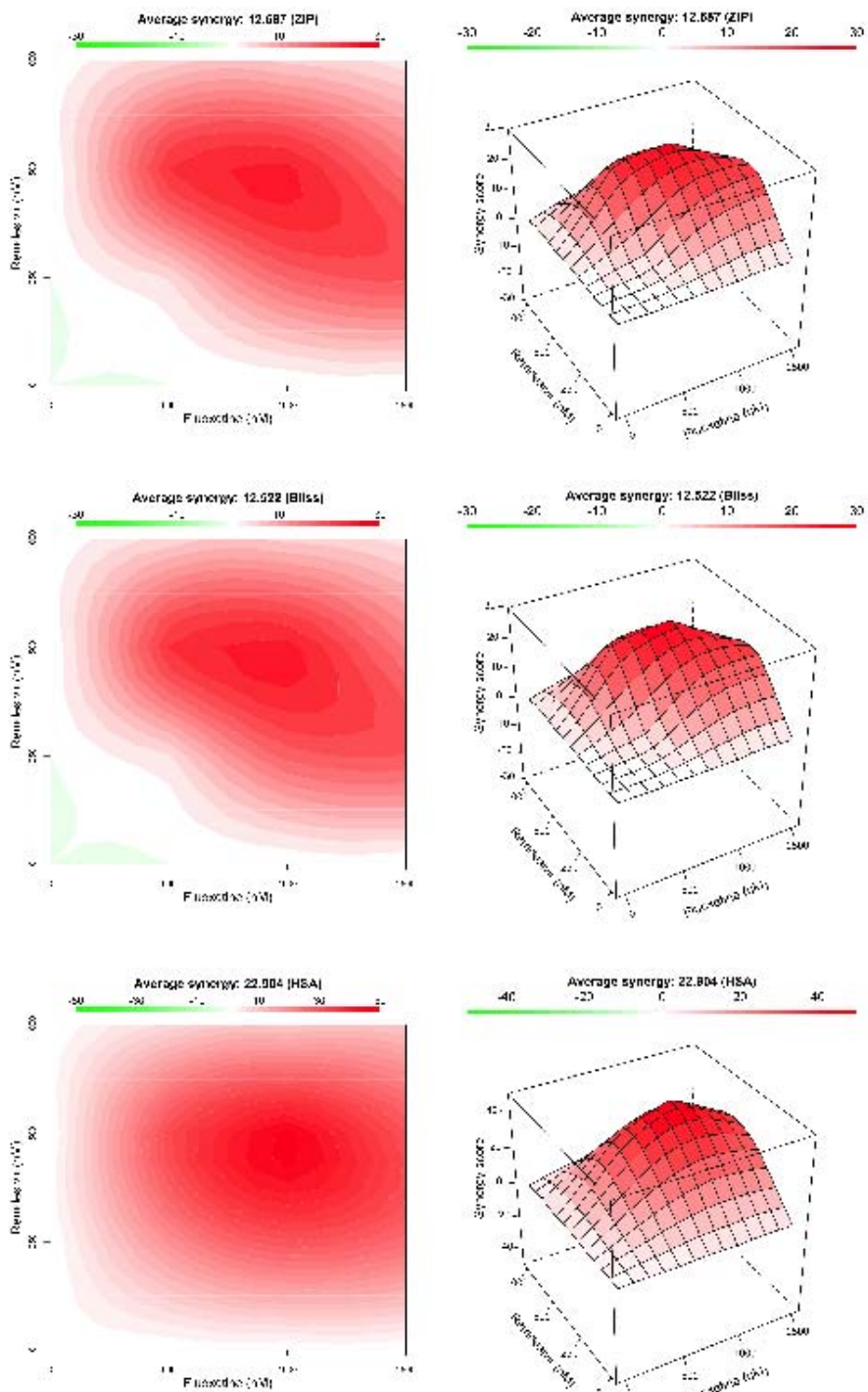
216 We, next considered the pharmacological interactions of the respective drug pairs. Thus, we
217 evaluated the drug interactions via Bliss independence, Highest single agent (HSA), and
218 ZIP, three commonly used reference synergy models that differ in their basic assumptions of
219 drug interaction they are based on. The results, presented in Figs. 4 and 5, consistently
220 argued for synergistic action of remdesivir with itraconazole and fluoxetine, as indicated by
221 the positive average synergy score across all models. Closer inspection of the drug
222 interaction relationships and landscape visualizations revealed that for ItraRem, the highest
223 synergy scores were calculated with the lower concentration ranges of both drugs (Fig. 4).
224 The strong synergy led to an overall drug combination sensitivity score (CSS) of 89.64,
225 resulting in >90% inhibition already at 500 nM of remdesivir and 250 nM of itraconazole.
226 FluoRem combination treatment had a higher average synergy score, as well as a higher
227 CSS score than ItraRem (92.82 vs 89.64), suggesting that this drug combination is more
228 likely to show synergy. Importantly, for all models, the FluoRem combinations that met the \geq
229 90% inhibition criterion were well within the high synergy area (Fig. 5).



230

Figure

231 **FIGURE 4.** Evaluation of the pharmacological interactions of itraconazole and remdesivir
232 (ItraRem). ZIP, Bliss independence, and Highest single agent (HSA) reference models were
233 used to assess the interaction landscapes. Interaction surfaces are color-coded according to
234 the synergy scores of the responses.



235
236 **FIGURE 5.** Evaluation of the pharmacological interactions of fluoxetine and remdesivir
237 (FluoRem). ZIP, Bliss independence, and Highest single agent (HSA) reference models
238 were used to assess the interaction landscapes. Interaction surfaces are color-coded
239 according to the synergy scores of the responses.

240 **4. DISCUSSION**

241 The nucleoside analog remdesivir with broad-spectrum antiviral activity against a range of
242 viruses including Ebola, Marburg, MERS, and SARS inhibits viral RNA polymerase and is
243 also active against SARS-CoV-2 (Warren et al., 2016; Sheahan et al., 2017, 2020; Agostini
244 et al., 2018; Brown et al., 2019). Indeed, remdesivir was the first new drug to receive an
245 FDA emergency use authorization for the treatment of severe COVID-19 cases. However, a
246 common concern about virus-directed antivirals is the development of drug resistance. Due
247 to their error-prone replication mode, drug-resistant viruses are increasingly encountered
248 (Strasfeld and Chou, 2010), as observed with the influenza neuraminidase inhibitor
249 oseltamivir (Kim et al., 2013). Because profound changes would be required to allow viruses
250 to replicate independently of otherwise essential host factors, the development of
251 host-directed therapeutics is an emerging concept. However, host-directed drugs will rather
252 cause impaired viral replication than complete eradication, thus demanding high drug
253 concentrations and starting treatment start as early as possible and for extended durations,
254 which is often associated with poor patient compliance. Because of these shortcomings,
255 combinatory treatments with both virus- and host-directed drugs are explored for enhanced
256 treatment success.

257 Enveloped viruses such as SARS-CoV-2 depend on the fusion of their lipid hull with the host
258 membrane to get access to the cytosol. The SARS-CoV-2 spike protein, which protrudes
259 from the virus surface, mediates initial binding to angiotensin-converting enzyme 2 (ACE2),
260 which serves as the host cell surface receptor (Li et al., 2003; Lan et al., 2020; Ou et al.,
261 2020; Zhou et al., 2020). To promote fusion with the host cell membrane, the spike protein
262 needs to be primed by proteolytic cleavage, which can be mediated by several host
263 proteases. Transmembrane protease serine 2 (TMPRSS2)-mediated cleavage leads to
264 fusion with the plasma membrane, while endosome-residing proteases are utilized by
265 endocytosed SARS-CoV-2 particles for fusion within endosomes. Since both routes have
266 been reported to contribute to the SARS-CoV-2 infectivity (Hoffmann et al., 2020), the
267 endosomal compartment is also a critical host/pathogen interface for SARS-CoV-2. Our
268 previous studies strongly support the late endosomal cholesterol balance as a cellular target

269 for antiviral intervention (Musiol et al., 2013; Kühnl et al., 2018; Schloer et al., 2019, 2020a,
270 2020b). Notably, endolysosomal lipid storage and cholesterol build-up could be induced via
271 repurposing of drugs approved for unrelated applications. We found that the triazole
272 derivative itraconazole, a clinically licensed antifungal drug (Organization, 2019) that directly
273 inhibits the endosomal cholesterol transporter NPC1 (Trinh et al., 2017) has an antiviral
274 potential on the endosomal fusion of enveloped viruses including influenza viruses (Schloer
275 et al., 2019). The findings presented in this study add SARS-CoV-2 to the spectrum of
276 itraconazole-sensitive enveloped viruses. Our results reveal a potent antiviral activity of
277 itraconazole on the production of SARS-CoV-2 infectious particles, with EC₅₀ values
278 comparable to what we previously reported for itraconazole-mediated antiviral activity
279 against IAV subtypes. The bioavailability after oral application of itraconazole is low because
280 of the low water solubility of this compound (Grant Prentice and Glasmacher, 2005;
281 Domínguez-Gil Hurlé et al., 2006). Only limited amounts are absorbed from the
282 gastrointestinal tract after ionization, and levels depend on the individual gastric acidity (Shin
283 et al., 2004; Domínguez-Gil Hurlé et al., 2006; Bae et al., 2011; Lestner and Hope, 2013;
284 Allegra et al., 2017). However, our previous study revealed a beneficial antiviral activity in
285 vivo (Schloer et al., 2019).

286 We recently discovered that the widely used antidepressant fluoxetine has strong
287 SARS-CoV-2 antiviral activity (Schloer et al., 2020a). Together with the findings presented
288 here on the inhibitory function of itraconazole treatment on SARS-CoV-2 replication, these
289 results suggest that both drugs are promising candidates for repurposing as a host-directed
290 drug for SARS-CoV-2 infection treatment. Both drugs most likely interfere with the proper
291 endosomal cholesterol levels. Whereas itraconazole and posaconazole both directly inhibit
292 the endosomal cholesterol transporter NPC1 (Trinh et al., 2017), fluoxetine functionally
293 blocks the endolysosome-residing enzyme sphingomyelin phosphodiesterase ("acid
294 sphingomyelinase", ASM), which in turn causes sphingomyelin accumulation and negatively
295 affects cholesterol release from this compartment (Kornhuber et al., 2010).

296 **5. CONCLUSION**

297 While remdesivir and the host-directed drugs itraconazole or fluoxetine target independent
298 pathways, we found that drug combinations together with remdesivir (ItraRem and
299 FluoRem) showed stronger antiviral activities against SARS-CoV-2 than the remdesivir
300 monotherapy. Moreover, the overall therapeutic effect of the combinations was larger than
301 the expected sum of the independent drug effects. Our analysis on the antiviral activity of
302 combinatory drug combinations via commonly used interaction models argue for an
303 enhanced efficacy that is based on synergistic drug interaction and suggests promising
304 novel options for SARS-CoV-2 treatment.

305 **ACKNOWLEDGEMENTS**

306 We thank Jonathan Hentrey for help with the plaque assays.

307 **FUNDING**

308 This research was funded by grants from the German Research Foundation (DFG),
309 CRC1009 “Breaking Barriers”, Project A06 (to U.R.) and B02 (to S.L.), CRC 1348 “Dynamic
310 Cellular Interfaces”, Project A11 (to U.R.), DFG Lu477/23-1 (to S.L.), the European
311 Research Council No. 716063 (to SZ and JT), the Academy of Finland No. 317680 (to SZ
312 and JT), the Interdisciplinary Center for Clinical Research (IZKF) of the Münster Medical
313 School, grant number Re2/022/20 (to U.R.) and from the Innovative Medizinische
314 Forschung (IMF) of the Münster Medical School, grant number SC121912 (to S.S.). S.S.,
315 S.L., and U.R. are members of the German FluResearchNet, a nationwide research network
316 on zoonotic influenza.

317 **CONFLICT OF INTEREST**

318 The authors declare no conflict of interest. The funders had no role in the design of the
319 study; in the collection, analyses, or interpretation of data; in the writing of the manuscript, or
320 in the decision to publish the results.

321 **AUTHOR CONTRIBUTIONS**

322 Conceptualization and methodology, S.S., U.R.; validation, formal analysis, investigation,
323 data curation, S.S., J.T., U.R.; resources, J.T., S.L.; U.R.; writing—original draft preparation,
324 U.R.; writing—review and editing, S.S., S.L., U.R.; visualization, S.S.; supervision, U.R.,
325 S.L., project administration, U.R.; funding acquisition, U.R. All authors have read and agreed
326 to the published version of the manuscript.

327 **REFERENCES**

328 Agostini, M.L., Andres, E.L., Sims, A.C., Graham, R.L., Sheahan, T.P., Lu, X., et al. (2018).
329 Coronavirus susceptibility to the antiviral remdesivir (GS-5734) is mediated by the viral
330 polymerase and the proofreading exoribonuclease. *MBio* 9: 2020.

331 Allegra, S., Fatiguso, G., Francia, S. De, Favata, F., Pirro, E., Carcieri, C., et al. (2017).
332 Evaluation of posaconazole pharmacokinetics in adult patients with invasive fungal
333 infection. *Biomedicines* 5:.

334 Bae, S.K., Park, S.-J., Shim, E.-J., Mun, J.-H., Kim, E.-Y., Shin, J.-G., et al. (2011).
335 Increased Oral Bioavailability of Itraconazole and Its Active Metabolite,
336 7-Hydroxyitraconazole, When Coadministered With a Vitamin C Beverage in Healthy
337 Participants. *J. Clin. Pharmacol.* 51: 444–451.

338 Baud, D., Qi, X., Nielsen-Saines, K., Musso, D., Pomar, L., and Favre, G. (2020). Real
339 estimates of mortality following COVID-19 infection. *Lancet Infect. Dis.* 20: 773.

340 Brown, A.J., Won, J.J., Graham, R.L., Dinnon, K.H., Sims, A.C., Feng, J.Y., et al. (2019).
341 Broad spectrum antiviral remdesivir inhibits human endemic and zoonotic
342 deltacoronaviruses with a highly divergent RNA dependent RNA polymerase. *Antiviral
343 Res.* 169:.

344 Domínguez-Gil Hurlé, A., Sánchez Navarro, A., and García Sánchez, M.J. (2006).
345 Therapeutic drug monitoring of itraconazole and the relevance of pharmacokinetic
346 interactions. *Clin. Microbiol. Infect.* 12: 97–106.

347 Faul, F., Erdfelder, E., Lang, A.-G., and Buchner, A. (2007). G*Power 3: A flexible statistical
348 power analysis program for the social, behavioral, and biomedical sciences. *Behav.*
349 *Res. Methods* 39: 175–191.

350 Fierabracci, A., Arena, A., and Rossi, P. (2020). COVID-19: A review on diagnosis,
351 treatment, and prophylaxis. *Int. J. Mol. Sci.* 21: 1–16.

352 Gordon, C.J., Tchesnokov, E.P., Woolner, E., Perry, J.K., Feng, J.Y., Porter, D.P., et al.
353 (2020). Remdesivir is a direct-acting antiviral that inhibits RNA-dependent RNA
354 polymerase from severe acute respiratory syndrome coronavirus 2 with high potency. *J.*
355 *Biol. Chem.* 295: 6785–6797.

356 Grant Prentice, A., and Glasmacher, A. (2005). Making sense of itraconazole
357 pharmacokinetics. *J. Antimicrob. Chemother.* 56: 17–22.

358 He, L., Kulesskiy, E., Saarela, J., Turunen, L., Wennerberg, K., Aittokallio, T., et al. (2018).
359 Methods for high-throughput drug combination screening and synergy scoring. In
360 *Methods in Molecular Biology*, (Humana Press Inc.), pp 351–398.

361 Hoffmann, M., Kleine-Weber, H., Schroeder, S., Krüger, N., Herrler, T., Erichsen, S., et al.
362 (2020). SARS-CoV-2 Cell Entry Depends on ACE2 and TMPRSS2 and Is Blocked by a
363 Clinically Proven Protease Inhibitor. *Cell* 181: 271–280.e8.

364 Ianevski, A., He, L., Aittokallio, T., and Tang, J. (2017). SynergyFinder: A web application for
365 analyzing drug combination dose-response matrix data. *Bioinformatics* 33: 2413–2415.

366 Ianevski, A., Yao, R., Fenstad, M.H., Biza, S., Zusinaite, E., Reisberg, T., et al. (2020).
367 Potential antiviral options against SARS-CoV-2 infection. *Viruses* 12:.

368 Kim, J.H., Resende, R., Wennekes, T., Chen, H.M., Bance, N., Buchini, S., et al. (2013).
369 Mechanism-based covalent neuraminidase inhibitors with broad-spectrum influenza
370 antiviral activity. *Science* (80-). 340: 71–75.

371 Kornhuber, J., Tripal, P., Reichel, M., Mühle, C., Rhein, C., Muehlbacher, M., et al. (2010).
372 Functional Inhibitors of Acid Sphingomyelinase (FIASMAs): A Novel Pharmacological
373 Group of Drugs with Broad Clinical Applications.

374 Kühnl, A., Musiol, A., Heitzig, N., Johnson, D.E., Ehrhardt, C., Grewal, T., et al. (2018). Late
375 endosomal/lysosomal cholesterol accumulation is a host cell-protective mechanism
376 inhibiting endosomal release of influenza A virus. *MBio* 9: e01345-18.

377 Lan, J., Ge, J., Yu, J., Shan, S., Zhou, H., Fan, S., et al. (2020). Structure of the
378 SARS-CoV-2 spike receptor-binding domain bound to the ACE2 receptor. *Nature* 581:
379 215–220.

380 Lestner, J., and Hope, W.W. (2013). Itraconazole: An update on pharmacology and clinical
381 use for treatment of invasive and allergic fungal infections. *Expert Opin. Drug Metab.*
382 *Toxicol.* 9: 911–926.

383 Li, W., Moore, M.J., Vasllieva, N., Sui, J., Wong, S.K., Berne, M.A., et al. (2003).
384 Angiotensin-converting enzyme 2 is a functional receptor for the SARS coronavirus.
385 *Nature* 426: 450–454.

386 Malyutina, A., Majumder, M.M., Wang, W., Pessia, A., Heckman, C.A., and Tang, J. (2019).
387 Drug combination sensitivity scoring facilitates the discovery of synergistic and
388 efficacious drug combinations in cancer. *PLoS Comput. Biol.* 15:

389 Musiol, A., Gran, S., Ehrhardt, C., Ludwig, S., Grewal, T., Gerke, V., et al. (2013). Annexin
390 A6-balanced late endosomal cholesterol controls influenza a replication and
391 propagation. *MBio* 4: 1–11.

392 Organization, W.H. (2019). World Health Organization Model List of Essential Medicines
393 (Geneve).

394 Ou, X., Liu, Y., Lei, X., Li, P., Mi, D., Ren, L., et al. (2020). Characterization of spike

395 glycoprotein of SARS-CoV-2 on virus entry and its immune cross-reactivity with
396 SARS-CoV. *Nat. Commun.* 11: 1–12.

397 Pruijssers, A.J., George, A.S., Schäfer, A., Leist, S.R., Gralinski, L.E., Dinnon, K.H., et al.
398 (2020). Remdesivir Inhibits SARS-CoV-2 in Human Lung Cells and Chimeric
399 SARS-CoV Expressing the SARS-CoV-2 RNA Polymerase in Mice. *Cell Rep.* 32:
400 107940.

401 Pushpakom, S., Iorio, F., Eyers, P.A., Escott, K.J., Hopper, S., Wells, A., et al. (2018). Drug
402 repurposing: Progress, challenges and recommendations. *Nat. Rev. Drug Discov.* 18:
403 41–58.

404 Rajgor, D.D., Lee, M.H., Archuleta, S., Bagdasarian, N., and Quek, S.C. (2020). The many
405 estimates of the COVID-19 case fatality rate. *Lancet Infect. Dis.* 20: 776–777.

406 Schloer, S., Brunotte, L., Goretzko, J., Mecate-Zambrano, A., Korthals, N., Gerke, V., et al.
407 (2020a). Targeting the endolysosomal host-SARS-CoV-2 interface by clinically licensed
408 functional inhibitors of acid sphingomyelinase (FIASMA) including the antidepressant
409 fluoxetine. *Emerg. Microbes Infect.* 1–26.

410 Schloer, S., Goretzko, J., Kühnl, A., Brunotte, L., Ludwig, S., and Rescher, U. (2019). The
411 clinically licensed antifungal drug itraconazole inhibits influenza virus *in vitro* and *in vivo*.
412 *Emerg. Microbes Infect.* 8: 80–93.

413 Schloer, S., Goretzko, J., Pleschka, S., Ludwig, S., and Rescher, U. (2020b). Combinatory
414 Treatment with Oseltamivir and Itraconazole Targeting Both Virus and Host Factors in
415 Influenza A Virus Infection. *Viruses* 12: 703.

416 Schwegmann, A., and Brombacher, F. (2008). Host-directed drug targeting of factors
417 hijacked by pathogens. *Sci. Signal.* 1: re8.

418 Sheahan, T.P., Sims, A.C., Graham, R.L., Menachery, V.D., Gralinski, L.E., Case, J.B., et al.

419 (2017). Broad-spectrum antiviral GS-5734 inhibits both epidemic and zoonotic
420 coronaviruses. *Sci. Transl. Med.* 9:.

421 Sheahan, T.P., Sims, A.C., Leist, S.R., Schäfer, A., Won, J., Brown, A.J., et al. (2020).
422 Comparative therapeutic efficacy of remdesivir and combination lopinavir, ritonavir, and
423 interferon beta against MERS-CoV. *Nat. Commun.* 11: 1–14.

424 Shin, J.H., Choi, K.Y., Kim, Y.C., and Lee, M.G. (2004). Dose-Dependent Pharmacokinetics
425 of Itraconazole after Intravenous or Oral Administration to Rats: Intestinal First-Pass
426 Effect. *Antimicrob. Agents Chemother.* 48: 1756–1762.

427 Strasfeld, L., and Chou, S. (2010). Antiviral drug resistance: Mechanisms and clinical
428 implications. *Infect. Dis. Clin. North Am.* 24: 809–833.

429 Tang, T., Bidon, M., Jaimes, J.A., Whittaker, G.R., and Daniel, S. (2020). Coronavirus
430 membrane fusion mechanism offers a potential target for antiviral development.
431 *Antiviral Res.* 178:.

432 Trinh, M.N., Lu, F., Li, X., Das, A., Liang, Q., Brabander, J.K. De, et al. (2017). Triazoles
433 inhibit cholesterol export from lysosomes by binding to NPC1. *Proc. Natl. Acad. Sci.*
434 114: 89–94.

435 Warren, T.K., Jordan, R., Lo, M.K., Ray, A.S., Mackman, R.L., Soloveva, V., et al. (2016).
436 Therapeutic efficacy of the small molecule GS-5734 against Ebola virus in rhesus
437 monkeys. *Nature* 531: 381–385.

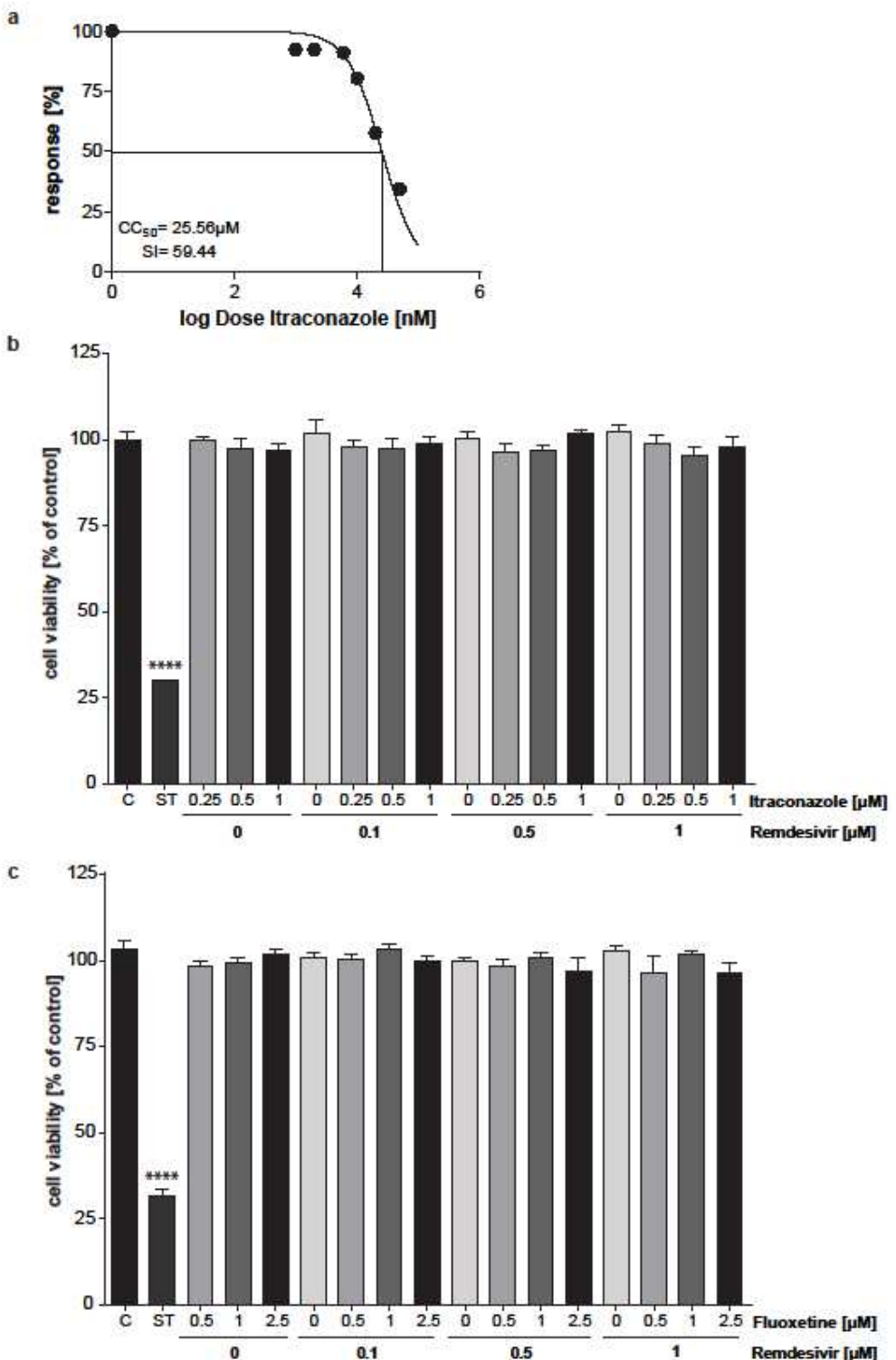
438 Wu, J.T., Leung, K., Bushman, M., Kishore, N., Niehus, R., Salazar, P.M. de, et al. (2020).
439 Estimating clinical severity of COVID-19 from the transmission dynamics in Wuhan,
440 China. *Nat. Med.* 26: 506–510.

441 Zhou, P., Yang, X. Lou, Wang, X.G., Hu, B., Zhang, L., Zhang, W., et al. (2020). A
442 pneumonia outbreak associated with a new coronavirus of probable bat origin. *Nature*

443 579: 270–273.

444 Zumla, A., Hui, D.S., Azhar, E.I., Memish, Z.A., and Maeurer, M. (2020). Reducing mortality
445 from 2019-nCoV: host-directed therapies should be an option. Lancet 395: e35–e36.

446 **SUPPORTING INFORMATION**

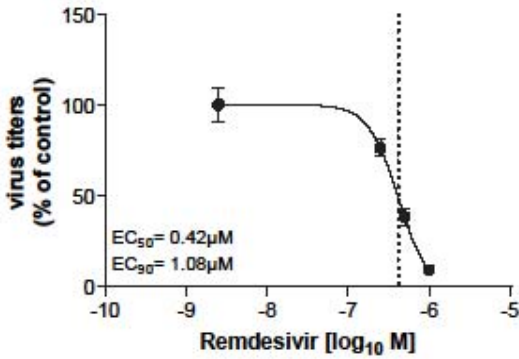


447

448 **SUPPORTING FIGURE 1** Analysis of the cytotoxicity of treatments. (a) Itraconazole, (b)

449 ItraRem, and (c) FluoRem combinatory treatment. Calu-3 cells were treated with the

450 indicated drug combinations for 48 h. Bars display mean percentages of viable
451 cells \pm SEM, with mean viability in solvent-treated control cells (C) set to 100%.
452 Staurosporine (ST)- induced cytotoxicity served as a positive control. $n=5$, one-way
453 ANOVA followed by Dunnett's multiple comparison test, $****p < 0.0001$.



454

455 **SUPPORTING FIGURE 2** Analysis Dose-Response curve of remdesivir treatments in
456 Calu-3 cells. Calu-3 cells were infected with 0.1 MOI of SARS-CoV-2 for 1 h and treated with
457 the indicated drug combinations for 48 h. Mean percent inhibition \pm SEM of SARS-CoV-2
458 replication, with mean virus titer in control cells (treated with the solvent DMSO) set to 100%;
459 $n=5$. LogEC₅₀ and LogEC₉₀ values were determined by fitting a non-linear regression
460 model. (Calu-3: EC50 = 0.42 μM, EC90 = 1.08 μM).